

# A constitutive model for sands: Evaluation of predictive capability

## Un modelo constitutivo para arenas: Evaluación de capacidad predictiva

A. Sfriso  
*University of Buenos Aires*

### RESUMEN

Se presenta un modelo constitutivo que describe el comportamiento mecánico de arenas bajo carga monótonica dentro del rango de tensiones y deformaciones de interés ingenieril. Utiliza elasticidad dependiente de la presión, una versión de tres invariantes del criterio de Murata–Miura para compresión plástica, un criterio de Matsuoka–Nakai extendido para la respuesta inelástica al corte, y una implementación 3D de la teoría tensión – dilatación de Rowe. Con el fin que el modelo sea útil y atractivo para los ingenieros geotécnicos, sus ocho parámetros fueron elegidos entre aquellos mejor conocidos por la comunidad geotécnica. Se presentan algunas simulaciones numéricas que comparan el desempeño del modelo con resultados experimentales.

Palabras clave: modelos constitutivos, tensión-dilatancia, arenas, ruptura de partículas

### ABSTRACT

A constitutive model to describe the mechanical behavior of sands under monotonic loading throughout the stress and strain range of engineering interest is presented. The model uses pressure-dependent elasticity, a three-invariant version of the Murata-Miura yield loci for plastic compression, an enhanced Matsuoka-Nakai criterion for inelastic shear response, and a 3D implementation of Rowe's stress-dilatancy theory. In order to make the model useful and attractive to geotechnical engineers, its eight parameters were selected among those well known to the geotechnical community. Some numerical simulations are presented to compare the model's performance against experimental results.

Keywords: constitutive modeling, strength-dilatancy, sands, particle crushing

### 1 INTRODUCTION

Computational geomechanics is gaining widespread acceptance as a reliable procedure for routine engineering analysis in both static and cyclic loading conditions. Mohr-Coulomb and hyperbolic laws are those most used by practitioners to model sand behavior, despite the fact that these models have input parameters that are problem-dependent. For instance, one set of parameters is used to model the behavior of the sand surrounding a pile shaft, and a different set is used to model the pile tip, even if shaft and tip rest in the same sand deposit.

Robust and reliable modeling of sand behavior may be better achieved if routine computational geomechanics benefits from some improvements included in advanced models available in the academic environment. These “advanced” features are well-known to practitioners and routinely accounted for in hand-made computations. Some of them are:

i) different plane strain and triaxial compression friction angles; ii) pressure dependent peak friction angle; iii) effects of particle crushing; iv) different dilatancy ratios in compression and extension tests; and v) the possibility that a sand specimen has to be both heavily overconsolidated and contractive, or normally consolidated and dilatant.

The success of a novel constitutive model designed for routine analysis can be ultimately measured by its degree of usage and, by the time it is introduced to the geomechanics community, by its ease to be understood and accepted. The most important decision that a model-builder can make to achieve this objective is to select few, easily understandable input parameters and use well established formulas wherever applicable.

The model presented here is the monotonic subset of a more general constitutive model for sands called ARENA and developed at the University of Buenos Aires, Argentina.

## 2 MODEL FORMULATION

### 2.1 Elasticity

Isotropic, pressure and void ratio dependent hypo-elasticity is adopted. Expressions proposed by Pestana (Pestana&Whittle 1995) and Hardin (Hardin&Richart 1963) were selected because they have material parameters not dependent on pressure or void ratio. These are

$$\begin{aligned} K &= c_b \frac{1+e_0}{e_0} \left( \frac{p}{p_{ref}} \right)^m p_{ref} \\ G &= c_s \frac{(c_e - e_0)^2}{1+e_0} \left( \frac{p}{p_{ref}} \right)^m p_{ref} \end{aligned} \quad (1)$$

where  $K$  is bulk modulus,  $G$  is shear modulus,  $c_b$ ,  $c_s$ ,  $c_e$ , and  $m$  are material parameters,  $p$  is mean pressure and  $p_{ref}$  is a reference pressure.  $e_0$  is the zero-stress void ratio, obtained by an elastic unload from current void ratio  $e$  to  $p = 0$  KPa.

$$e_0 = e \exp \left[ \frac{1}{c_b (1-m)} \left( \frac{p}{p_{ref}} \right)^{1-m} \right] \quad (2)$$

### 2.2 Sources of inelasticity

The mechanical behavior of sands depends mainly on the resistance of particle contacts to sliding in shear and crushing in compression.

While the physical phenomena that governs both deformation mechanisms are inter-linked and not perfectly understood, the conceptual problem can be splitted for modeling purposes into the effects of shear at constant mean pressure and proportional compression.

#### 2.2.1 Shear loading

In a typical triaxial test, deformation in shear is governed by the change of stress-ratio, measured in tensor  $\mathbf{r} = \mathbf{s}/p$  or scalar form  $r = \|\mathbf{r}\|$ .  $\mathbf{s} = \boldsymbol{\sigma} - p\mathbf{I}$  is the deviatoric stress tensor,  $\boldsymbol{\sigma}$  is the stress tensor and  $\mathbf{I}$  is the unit tensor. In general stress space, however, the obliquity of the stress state has no unique definition. One suitable scalar measure is the aperture of the Matsuoka–Nakai (Matsuoka&Nakai 1974) cone

$$M = 3 \frac{r^2 - 3J_{3r}}{1 - \frac{1}{2}r^2 + J_{3r}} \quad (3)$$

where  $J_{3r} = \frac{1}{3} \mathbf{r} \cdot \mathbf{r} \cdot \mathbf{r}$ . For hydrostatic conditions (no shear stress),  $r = J_{3r} = M = 0$ .

#### 2.2.2 Proportional compression

In a typical oedometer compression test all stresses grow proportionally, forcing particles to slide, roll and crush to a more dense packing. The relevant stress measure is the major principal stress  $\sigma_1$  but, if the stress ratio is known,  $p$  can be used as a more convenient stress measure. In a general compression test, however, obliquity varies during compression, and a cap closure must be used.

### 2.3 Effect of mean pressure on inelastic behavior

Both shear and compression behavior depend on mean pressure  $p$ , void ratio  $e$  and relative density  $D_r$  for a given sand. For extreme high stresses, an ultimate  $e - p$  relationship was determined by Pestana (Pestana&Whittle 1995) in the form

$$p_{ult} = e^{-1/\rho} p_r p_{ref} \quad (4)$$

where  $p_r$  and  $\rho$  are material parameters. Pestana (Pestana&Whittle 1995) shows that  $\rho$  lies in the range  $0.36 < \rho < 0.45$  for many sands. Because  $\rho$  has little influence in the behavior of sands at engineering stress levels, it is accurate enough to take  $\rho = 0.40$  and define the crushing parameter

$$\chi = \frac{p}{p_{ult}} = \frac{e_0^{2.5}}{p_r} \frac{p}{p_{ref}} \quad (5)$$

Thus, if  $\chi \ll 1$  particle crushing is negligible and both dilatancy and compression stiffness depend on relative density only. On the other side, if  $\chi \approx 1$ , no dilatancy occurs and compression behavior depends mainly on the strength of the grain material.

### 2.4 Shear strength

#### 2.4.1 Peak friction angle

Loose sands contract during drained shear until a critical void ratio  $e_c$  and a critical friction angle  $\phi_c$  are reached (Casagrande 1936, 1975). Dense sands dilate until they reach the same state  $\{e_c, \phi_c\}$  but, while dilating, the instant mobilized angle of friction is higher than  $\phi_c$  up to a peak value  $\phi_f$ .

Under high pressure, no dilation occurs and therefore  $\phi_f = \phi_c$  (De Beer 1965). Bolton (Bolton 1986) took into account the dependency of  $\phi_f$  on both stress and density through the expression

$$\phi_f = \phi_c + 3^\circ D_r \left( Q - \ln \left[ \frac{p}{\text{KPa}} \right] \right) - 3^\circ \quad (6)$$

Parameter  $Q$  accounts for particle strength. Crushing resistance of a given sand, however, depends both on particle strength and void ratio. This fact can be better accounted for with the modified expression

$$\phi_f = \phi_c - 3^\circ D_r \ln[\chi] - 2^\circ \quad (7)$$

Data used by Bolton (Bolton 1986) to calibrate (6) is matched by (7) within  $1.5^\circ$ . An upper limit for engineering analysis  $\phi_{max}$  is obtained by computing (7) with the minimum void ratio  $e_{min}$  and for a low pressure  $p=100$  KPa. Expression (7) predicts  $\phi_f < \phi_c$  if

$$p > \frac{p_r}{e_0^{2.5}} \exp\left[\frac{-2^\circ}{3^\circ D_r}\right] p_{ref} \quad (8)$$

which means that the sample must densify to reach  $\{e_c, \phi_c\}$ . If contraction is impeded, so-called liquefaction occurs.

#### 2.4.2 Failure surface in shear

$\phi_f$  is a parameter of the Mohr- Coulomb failure criterion. In the present model, the Matsuoka-Nakai criterion (Matsuoka&Nakai 1974) is adopted and  $\phi_f$  is used to calibrate it. The failure surface in shear is

$$F_f = \frac{\mu_f + 6}{2} r^2 - (\mu_f + 9) J_{3r} - \mu_f = 0 \quad (9)$$

where  $\mu_f = 8 \tan^2[\phi_f]$  is a strength parameter that inherits dependence on  $D_r$  and  $\chi$ .

The selection of a three invariant failure criterion like (9) accounts for the difference between plane strain and triaxial compression friction angles, whereas it's calibration using (7) accounts for the dependency of peak friction on density and mean pressure. Fig. 1 shows the failure surface in shear, while Fig. 2 shows the calibration of (7) for Sacramento sand (Lee 1967).

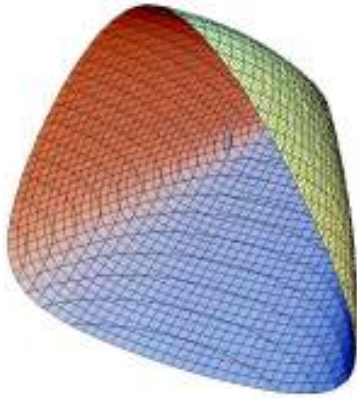


Fig. 1. Curved failure surface in shear, accounting for pressure, density and stress – path dependent peak friction angle.

### 2.5 Shear plasticity

#### 2.5.1 Loading surface and dev-plastic strain

The loading surface is the Matsuoka-Nakai cone passing through the current stress state

$$F_s = \frac{\mu + 6}{2} r^2 - (\mu + 9) J_{3r} - \mu = 0 \quad (10)$$

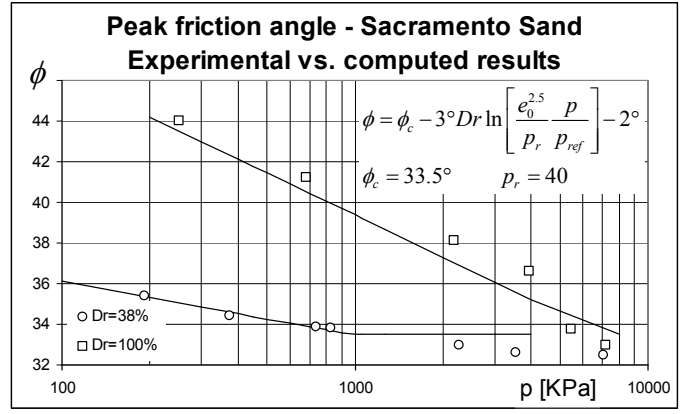


Fig 2. Calibration of (7) for Sacramento sand. Experimental data after Lee, 1967.

where  $\mu$  is an internal variable. The plastic strain increment in shear  $\dot{\mathbf{e}}_s^p = \dot{\lambda}_s \mathbf{m}_s$  is governed by the non-associative tensor field (Macari 1989)

$$\mathbf{m}_s = \frac{\mathbf{n}_s^d}{\|\mathbf{n}_s^d\|} + \beta \mathbf{I} \quad (11)$$

where  $\mathbf{n}_s^d = \mathbf{n}_s - \frac{1}{3} \mathbf{n}_s : \mathbf{\Pi}$ ,  $\mathbf{n}_s = \partial F_s / \partial \boldsymbol{\sigma}$ ,  $\beta$  is a dilatancy variable and  $\lambda_s$  is a plastic multiplier.

#### 2.5.2 Dilatancy

$\beta$  is computed after Rowe's strength-dilatancy theory (Rowe 1962). Rowe introduced the expression  $W_{in}/W_{out} = N_{cv}$ ,  $W_{in}$  and  $W_{out}$  being the work done by and against the surrounding media,  $N_{cv} = (1 + \sin \phi_{cv}) / (1 - \sin \phi_{cv})$  and  $\phi_{cv}$  the constant-volume friction angle.

Due to deviatoric associativity,  $\mathbf{m}_s$  shares eigenvectors with  $\boldsymbol{\sigma}$ , a fact that allows for the computation of  $\beta$  in their common principal stress space, where  $\boldsymbol{\sigma} \rightarrow \{\sigma_1, \sigma_2, \sigma_3\}$  and  $\mathbf{m}_s \rightarrow \{m_{s1}, m_{s2}, m_{s3}\}$ . The expressions are

$$W = \boldsymbol{\sigma} \cdot \mathbf{m}_s^d = \{\sigma_1 m_{s1}^d, \sigma_2 m_{s2}^d, \sigma_3 m_{s3}^d\}$$

$$\beta = \frac{\sum_{W_I > 0} W + N_{cv} \sum_{W_I < 0} W}{N_{cv} \sum_{W_I < 0} \sigma_I + \sum_{W_I > 0} \sigma_I} \quad I : 1 \dots 3 \quad (12)$$

$\phi_{cv}$  depends on mineralogy, density and particle shape. A convenient expression, following concepts by Horne (Horne 1965, 1969) and introduced here is

$$\phi_{cv} = \max \left\{ \begin{array}{l} \phi_c + (3^\circ D_r \ln[\chi] + 2^\circ) / 3 \\ 9/8 \phi_c - 8^\circ \end{array} \right. \quad (13)$$

These expressions account for contractive – dilatant behavior, lower  $\phi_{cv}$  values for dense samples and low confinement, and a distinct response in triaxial compression, plane strain and triaxial extension.

Fig. 3 shows the dilatancy coefficient  $\beta$  as a function of  $\sigma_1/\sigma_3$  and  $\sigma_2/\sigma_3$  ratios in the range 1 to 5, for the particular case  $N_{cv} = 3$ .

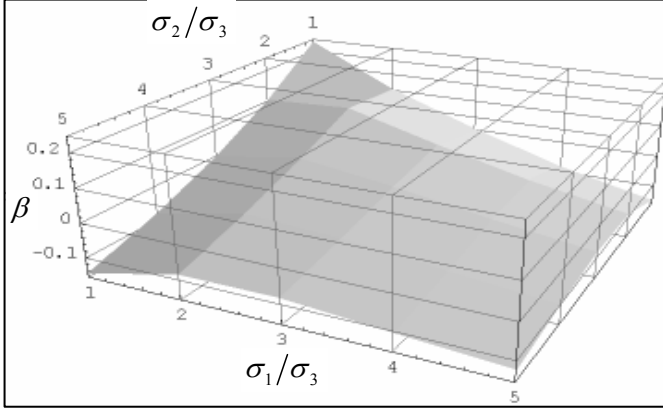


Fig. 3. Stress – ratio dependent dilatancy coefficient.

### 2.5.3 Hardening function in shear

Duncan-Chang's hyperbolic law (Duncan&Chang 1970) for monotonic loading is the most frequently used stress-strain law for sands. Applied to shear modulus it yields

$$G_t = G_i \left( 1 - R_f \frac{\sigma_1 - \sigma_3}{(\sigma_1 - \sigma_3)_f} \right)^2 \quad (14)$$

In (14),  $G_t$  is the tangent shear modulus,  $G_i$  is the "static initial" shear modulus, and  $R_f$  is the failure ratio (Duncan&Chang 1970, Duncan et al 1980, Nuñez 1995). The hyperbolic law can be adapted to the Matsuoka-Nakai criterion and converted to a hardening function for primary loading

$$\dot{\mu} = \frac{2\sqrt{3}}{\sqrt{\mu_f}} \frac{G_t/G}{1 + G_t/G} \frac{G}{p_s} \|\dot{\boldsymbol{\epsilon}}_s^{pd}\| \quad (15)$$

$$G_t = G_i \left( 1 - R_f \sqrt{\mu/\mu_f} \right)^2$$

In the above expression,  $G_i$  is pressure and density dependent, and a dedicated set of material parameters should be adopted to calibrate it. To avoid these extra parameters, concepts introduced by Trautmann and Kulhawy (Trautmann&Kulhawy 1987) can be exploited to get the relationships

$$G_i = \frac{1+2\Psi}{6} G \quad R_f = 0.7 + 0.2\Psi \quad (16)$$

where  $\Psi = (\tan \phi_f - \tan \phi_c) / (\tan \phi_{\max} - \tan \phi_c)$  is an indirect measure of stress level and density. Expressions (16) were calibrated to match data by Duncan (Duncan et al 1980) and Seed (Seed et al 1984). For instance, a dense sample under low stresses has a "initial static" to "elastic" stiffness ratio  $G_i/G \sim 1/2$  and a failure ratio  $R_f \sim 0.9$ , whereas the same sample under high stresses shows  $G_i/G \sim 1/5$  and  $R_f \sim 0.7$ .

## 2.6 Plastic compression

### 2.6.1 Yield surface

Murata and Miura (Murata&Miura 1989) proposed a closed yield surface for sands in the low and high pressure range. It's expression is

$$\left( (\sigma_1 - \sigma_3)/p \right)^2 + \eta_1 \ln[p/p_c] = 0 \quad (17)$$

where  $\eta_1$  is a material parameter and  $p_c$  is the pre-consolidation pressure. An alternative expression having a Matsuoka-Nakai shaped cross section, derived from Sfriso (Sfriso 1996), is

$$F_c = M + \eta \ln[p/p_c] = 0 \quad (18)$$

Fig. 4 shows a trimmed side and a front view of (18). Three slices have been cut from the latter to show the complete surface closing towards its apex.

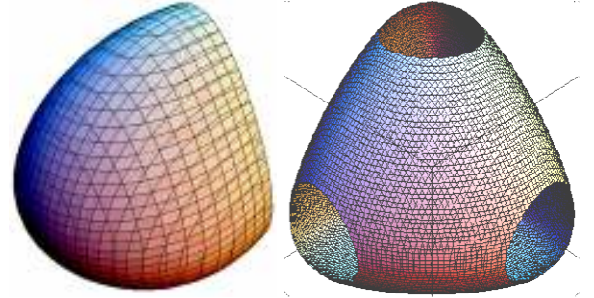


Fig 4. Partial side view and front view of the cap closure.

### 2.6.2 Plastic strains

Associative cap plasticity is adopted. Plastic strains in compression are computed using  $\dot{\boldsymbol{\epsilon}}_c^p = \dot{\lambda}_c \mathbf{m}_c$ , where  $\mathbf{m}_c = \mathbf{n}_c / \|\mathbf{n}_c\|$ ,  $\mathbf{n}_c = \partial F_c / \partial \boldsymbol{\sigma}$  and  $\dot{\lambda}_c$  is a plastic multiplier. While (17) was intended to model both shear and compression behavior of sands, (18) only serves as a cap closure. To avoid unrealistic dilatancy in proportional compression,  $\eta$  is solved out to yield  $\mathbf{I} : \mathbf{m}_c = 0$  at failure. The expression is

$$\eta = \frac{\mu_f}{12} \left( 3\mu_f + \sqrt{\mu_f} \sqrt{\mu_f + 8} + 24 \right) \quad (19)$$

The intersection between the cap closure (18) and the loading surface (10) is a planar curve entirely contained in a deviatoric plane in stress space.

### 2.6.3 Hardening function in compression

Relative density dominates low pressure stiffness in isotropic compression, while particle crushing is the driving mechanism in the high pressure range (Roberts&De Souza 1958, Schultze&Moussa 1961, Pestana&Whittle 1995). In this model, these two stress regions are modeled separately via distinct reduction factors  $C_l$  and  $C_h$  applied to the elastic bulk stiffness  $K^p = C_l / C_h K$ , namely

$$C_l = \frac{2-D_r}{D_r} \quad C_h = \frac{c_b}{2.5} \left( \frac{p}{p_{ref}} \right)^{m-1} - 1 \quad (20)$$

where  $l$  and  $h$  stand for low and high pressure. Intermediate response depends on the contribution of both mechanisms via a weighting function

$$\zeta = \frac{1}{2} + \frac{1}{2} \operatorname{erf} \left[ \sqrt{2} (1+D_r) (\chi-1) \right] \quad (21)$$

Oedometric compression and isotropic compression of a given sand yield approximately the same  $\sigma_I - \varepsilon_v$  curve. This allows for the extension of isotropic compression relationships to general stress space. The adopted hardening function in compression is

$$\dot{p}_c = \sqrt{3} \frac{1 - (\sqrt{M} \sqrt{M+8} - M)/6}{(1-\zeta)C_l + \zeta C_h} K \|\dot{\varepsilon}_c^p\| \quad (22)$$

### 2.7 Behavior in tension

No tensile stresses are allowed for. If a strain path leads to tensile stresses, the response is zero stress, zero stiffness and all internal variables are reset.

### 2.8 Input parameters

Input parameters are eight:  $e_{min}$  and  $e_{max}$ , min / max void ratios needed to compute  $D_r$ ;  $c_b$  and  $m$  for bulk stiffness;  $c_s$ ,  $c_e$  and  $m$  for shear stiffness,  $\phi_c$  for critical state friction angle and  $p_r$  for particle crushing. Of these, only  $c_b$  and  $p_r$ , adopted from Pestana's compression model, need some comment.  $p_r$  can be best calibrated using a series of triaxial compression tests of dense samples, performed over the maximum available pressure range, or estimated from available data on the dependence of peak friction angles on mean pressure (see, for instance, Duncan et al 1980).  $c_b$  can be readily computed from the rebound curve of an oedometer test of a dense sample, where plastic deformations developed during unloading are negligible. It can also be estimated from available data and correlations (see, for instance, Seed et al 1984).

## 3 MODEL IMPLEMENTATION

The model was integrated through a fully implicit, generalized plasticity algorithm in strain space. Details of the numerical issues have been presented elsewhere (Sfriso 2006a, b). The model was implemented in Plaxis V8.2 as an user-defined model. The *DLL* library and user manual is available for download at [www.fi.uba.ar/materias/6408](http://www.fi.uba.ar/materias/6408).

## 4 MODEL VALIDATION

Fig. 5 shows the predicted vs. measured behavior of Sacramento river sand in isotropic compression (Lee 1967). Adopted parameters are shown in the figure.

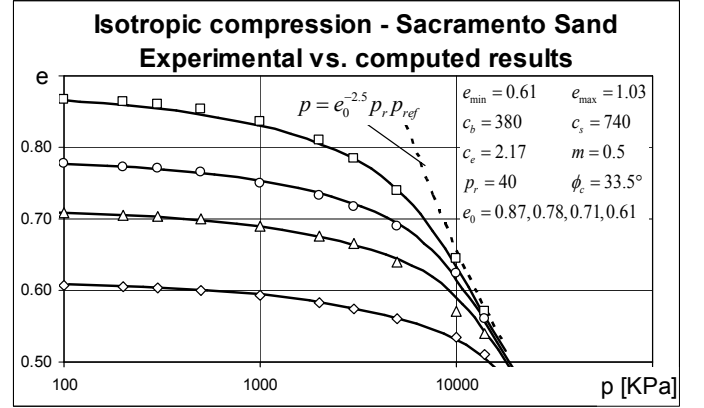


Fig. 5. Predicted vs. experimental results for Sacramento river sand in isotropic compression. Data from Lee, 1967.

Fig. 6 shows the numerical simulation of oedometer tests of normally consolidated Sacramento river sand, while Fig. 7 reproduces the simulation of the same tests on samples preconsolidated to  $\sigma_{Ic} = 100$  KPa. While no slope change is observed at  $\sigma_{Ic}$  for the densest OC sample, a clear change in overall stiffness is predicted for the loosest one.

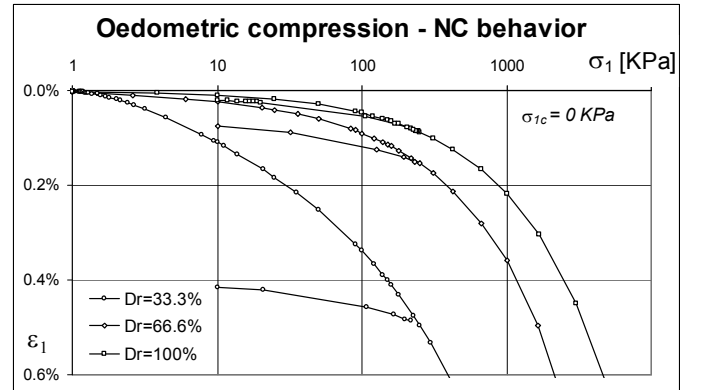


Fig. 6. Plaxis simulation of an oedometer test of a normally consolidated sample of Sacramento river sand.

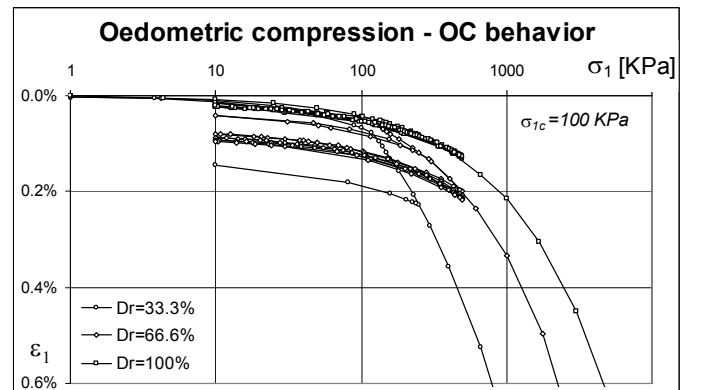


Fig. 7. Plaxis simulation of an oedometer test of a over consolidated sample of Sacramento river sand.

Fig. 8 shows the calibration of the model for the monotonic undrained shearing of Nevada Sand. Data was obtained from Arulmoni et al (Arulmoni et al 1992). Further information can be found elsewhere (Sfriso 2006a, b). The difference between the predicted and observed pore pressure response largely obeys to water cavitation in the experimental test.

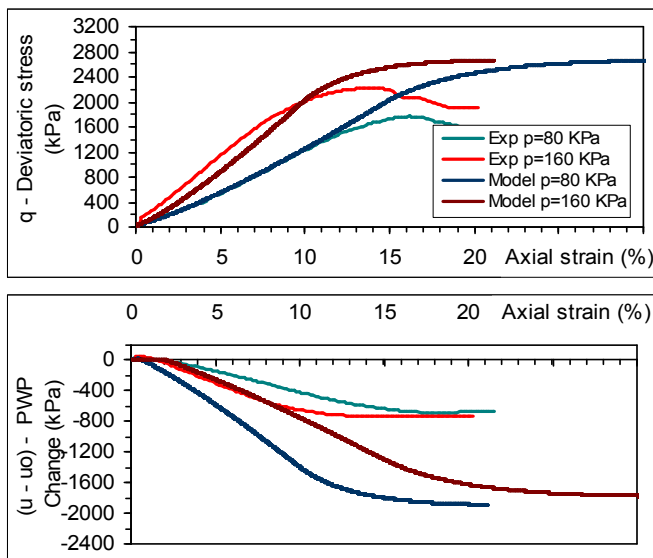


Fig. 8. Predicted and observed behavior of Nevada sand during undrained shearing. Data from Arulmoni et al, 1992.

## 5 CONCLUSIONS

A constitutive model for the monotonic behavior of sands has been presented. The model uses eight material parameters to account for many aspects that are not included in other models oriented to routine analyses, namely the effect of particle crushing on peak strength and compression stiffness and a 3D implementation of strength – dilatancy theory.

The model has been calibrated using widely accepted expressions by Hardin (Hardin&Richart 1963), Duncan (Duncan et al 1980) and Seed (Seed et al 1984). Parameters have been chosen, whenever possible, among those most accepted by geotechnical engineers. Most of them have large available databases gathered during decades of routine usage.

Despite the relatively few material parameters used, the model retains an acceptable degree of predictive capability for many problems, including the behavior of foundations and slopes.

## ACKNOWLEDGMENTS

The writer acknowledges the deep influence that Eduardo Núñez, master and advisor, had in this research project through many years of continuous teaching and guidance. Comments and support by E. Dvorkin, E. Macari, G. Etse and G. Weber are gratefully recognized.

## REFERENCES

- Arulmoni, K. et al (1992). VELACS Laboratory testing program. Soil data report. ETP 90-0562, 77 p.
- Bolton, M. (1986). The strength and dilatancy of sands. *Geotechnique* 36, 1, 65-78.
- Casagrande, A. (1936). Characteristics of cohesionless soils affecting the stability of slopes and earth fills. *J. Boston Soc. Civil Engineers*, 23 1, 13-32.
- Casagrande, A. (1975). Liquefaction and cyclic deformation of sands - a critical review. *V PCSMF*, 1-25. Buenos Aires.
- De Beer, E. (1965). Influence of the mean normal stress on the shearing resist. of sand. *VI ICSMF*, Montreal, 1, 165-169.
- Duncan, J. and C. Chang (1970). Nonlinear analysis of stress and strain in soils. *Journal of Soil Mechanics Foundation Division, ASCE*, 96, SM5, 1629-1653
- Duncan, J., P. Byrne, K. Wong and P. Mabry (1980). Strength, stress-strain and bulk modulus parameters for finite element analyses of stresses and movements in soil masses. Report UCB/GT/80-01, Berkeley, 72 p
- Hardin, B. and F. Richart (1963). Elastic wave velocities in granular soils. *Journal of Soil Mechanics Foundation Division, ASCE*, 89, SM1, 33-65.
- Horne, M. (1965). The behaviour of an assembly of rotund, rigid, cohesionless particles I, II. *Proc. Roy. Soc. London A*, 286, 68-97.
- Horne, M. (1969). The behaviour of an assembly of rotund, rigid, cohesionless particles III. *Proc. Roy. Soc. London A*, 310, 21-34.
- Lee, K. and H. B. Seed (1967). Drained strength characteristics of sands. *JSMFD, ASCE*, 93, SM6, 117-141.
- Macari, E. (1989). Behavior of granular materials in a reduced gravity environment and under low effective stresses. Ph. D Thesis, U. of Colorado, 177 p.
- Matsuoka, H. and T. Nakai (1974). Stress-deformation and strength characteristics of soil under three different principal stresses. *Proceedings of Japan Society of Civil Engineers*, 233, 59-70.
- Murata, H., N. Miura, M. Hyodo and N. Yasufuku (1989). Experimental study on yielding of sands. In: *Mechanics of granular materials*, Report ISSMFE TC13, 173-178.
- Núñez, E. (1995). Propiedades mecánicas de materiales granulares incoherentes *Acad. Nac. de Cs. Ex. Fis. Nat. Bs. As.*, 46, 71-89.
- Pestana, J. and A. Whittle (1995). Compression model for cohesionless soils. *Geotechnique*, 45(4), 611-631.
- Roberts, J. and J. De Souza (1958). The compressibility of sands, *Proceedings ASTM*, 58, 1269-1277.
- Rowe, P. (1962). The stress dilatancy relation for static equilibrium of an assembly of particles in contact. *Proc. Royal Soc. London*, 269, 500-527.
- Schultze, E. and A. Moussa (1961). Factors affecting the compressibility of sand, *Proceedings V International Conference on Soil Mechanics and Foundation Engineering, Paris*, I, 335-340.
- Seed, H., R. Wong, I. Idriss and K. Tokimatu (1984). Moduli and damping factors for dynamic analyses of cohesionless soils. Report UCB/EERC-84/14, Berkeley, 37 p.
- Sfriso, A. (1996). Una ecuación constitutiva para arenas. *Encuentro de geotécnicos argentinos GT'96,I*, 38-46.
- Sfriso, A. (2006a). Calibration of ARENA for Nevada sand based on VELACS project results. In: *VII WCCM*, electronic publication, Los Angeles.
- Sfriso, A. (2006b). ARENA – Una ecuación constitutiva para arenas. Dr. Eng. Thesis, submitted to Univ. of Buenos Aires.
- Trautmann, C. and F. Kulhawy (1987). CUFAD - A Computer program for compression and uplift foundation analysis and design. Report EL-4540-CCM, Vol 16. EPRI, 148 p.